ACS APPLIED NANO MATERIALS
Cite This: ACS Appl. Nano Mater. XXXX, XXX, XXX−XXX
Article
www.acsanm.org

Full-Color Scattering Based on Plasmon and Mie Resonances of Gold Nanoparticles Modulated by Fabry−Pérot Interference for Coloring and Image Projection

Hiroyasu Nishi* and Tetsu Tatsuma*

Institute of Industrial Science, The University of Tokyo, 4-6-1, Komaba, Meguro-ku, Tokyo 153-8505, Japan

Supporting Information

ABSTRACT: Plasmonic coloring of bulk materials has been based mostly on light absorption of metal nanoparticles. However, relatively large plasmonic nanoparticles also show unique scattering colors. Such scattering nanoparticles have been applied to dichroic and multichromatic materials. Among plasmonic materials, silver nanoparticles are suitable for full-color absorption and scattering. Even so, their stability is not necessarily sufficient for practical use, in particular when those are in contact with a semiconductor such as TiO_2, which is often used as a highly dielectric material. Although gold nanoparticles are more stable, those do not exhibit plasmon resonance in the blue color range. In this study, we achieved full-color scattering from gold nanoparticles by the aid of Mie scattering. Gold nanoparticles with a sufficient size were deposited on a thin TiO_2 layer, and their blue, green, and red scattering based on nonplasmonic Mie resonance, plasmonic full-surface mode, and plasmonic interface mode, respectively, were modulated on the basis of Fabry−Pérot interference by changing the TiO_2 thickness. The full-color scattering films would be used for anticounterfeiting. Their additional applications include a transparent projection screen. It looks almost transparent under ambient light, but full-color images can be displayed on the screen by a projector. The present materials are suitable for large-area applications because they are easy to be prepared through a chemical bottom-up technique.

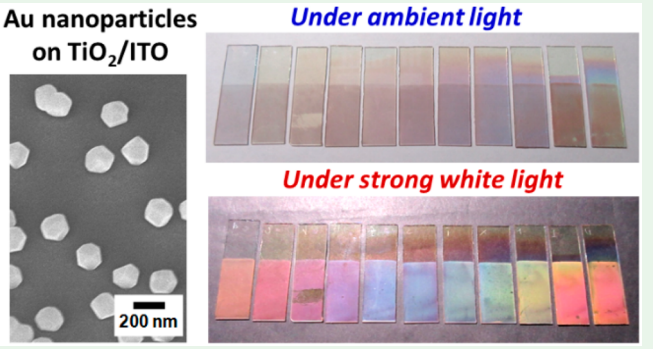

KEYWORDS: *localized surface plasmon resonance, Au nanoparticle, plasmonic coloring, light scattering, Mie scattering, Fabry−Pérot interference, transparent projection screen*

Downloaded via 46.148.127.37 on August 5, 2019 at 15:03:37 (UTC).
See https://pubs.acs.org/sharingguidelines for options on how to legitimately share published articles.

1. INTRODUCTION

Plasmonic coloring has fascinated us with vivid colors of metal nanoparticles. It is mostly based on wavelength-selective light absorption, which gives bright colors to transmitted light. Because metal nanoparticles have large absorption and scattering cross sections[1,2] and tunable resonance wavelength, which depends on metal species,[1,3] particle size,[2,4] shape,[1,5−7] and local environment,[8] they are suitable for elaborate coloring. Cutting edge plasmonic coloring with nanostructures prepared by laser ablation of metal surface and nanolithography, including metasurfaces, also has made good use of selective absorption or reflection.[9−16] Another coloring mechanism, which is unique to plasmonic nanomaterials, is wavelength-selective light scattering. It has allowed optical observation of single particles since Zhigmondy developed dark-field microscopy.[17] Even though the dark-field observation of nanoscale scattering has been used widely, plasmonic scattering is not used often for coloring of bulk materials.[18,19]

However, plasmonic scattering gives unique optical properties to materials such as glass. A typical example is the Lycurgus Cup,[20] which contains plasmonic Au−Ag alloy nanoparticles[21] and exhibits two different colors based on reddish transmitted light and greenish scattered light. We took advantage of site-selective excitation of plasmonic nanoparticles on a dielectric substrate[22,23] and developed trichromatic materials that show, for instance, blue scattered light, yellow reflected light, and red transmitted light.[22] It was also applied to asymmetric scattering films that exhibit, for example, blue scattered light for front incidence and red scattered light for back incidence.[22,24,25] In addition, site-selective etching of plasmonic nanoparticles on a semiconductor[26,27] by plasmon-induced charge separation (PICS)[28,29] allows photodrawing of multicolor scattering images and one-way visible translucent images.[30] Those unique scattering-based plasmonic coloring would be applied to optical materials, drawing images, and anticounterfeiting.

By adjusting the balance between the absorption and scattering, the material can be applied to transparent projection screens.[23,31−33] We developed a full-color scattering screen by tuning blue and yellow-red plasmonic scattering from Ag

Received: May 25, 2019
Accepted: July 22, 2019
Published: July 22, 2019

© XXXX American Chemical Society

DOI: 10.1021/acsanm.9b00990
ACS Appl. Nano Mater. XXXX, XXX, XXX−XXX

Scheme 1. Schematic Illustrations to Show (a) Fabrication Processes of Au Nanoparticle-Deposited Substrates and (b) Mechanisms of Multicolor Scattering from Au Nanoparticles

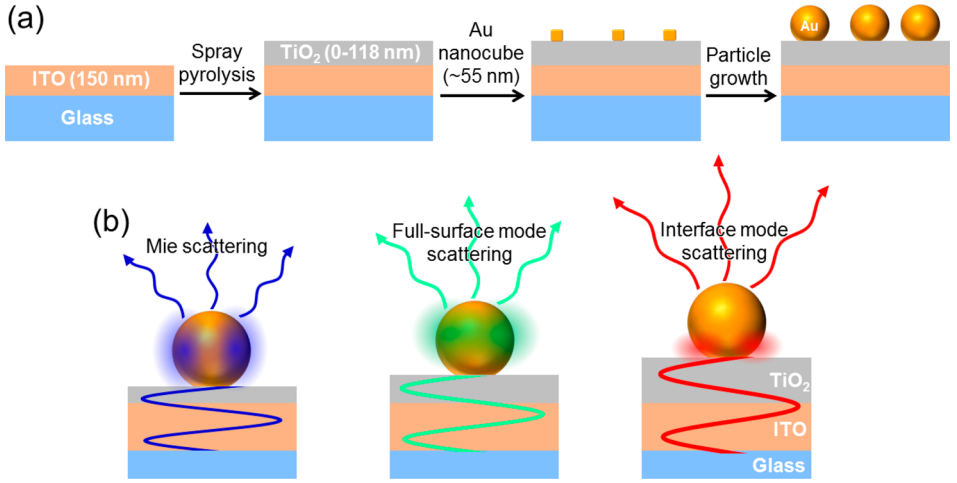

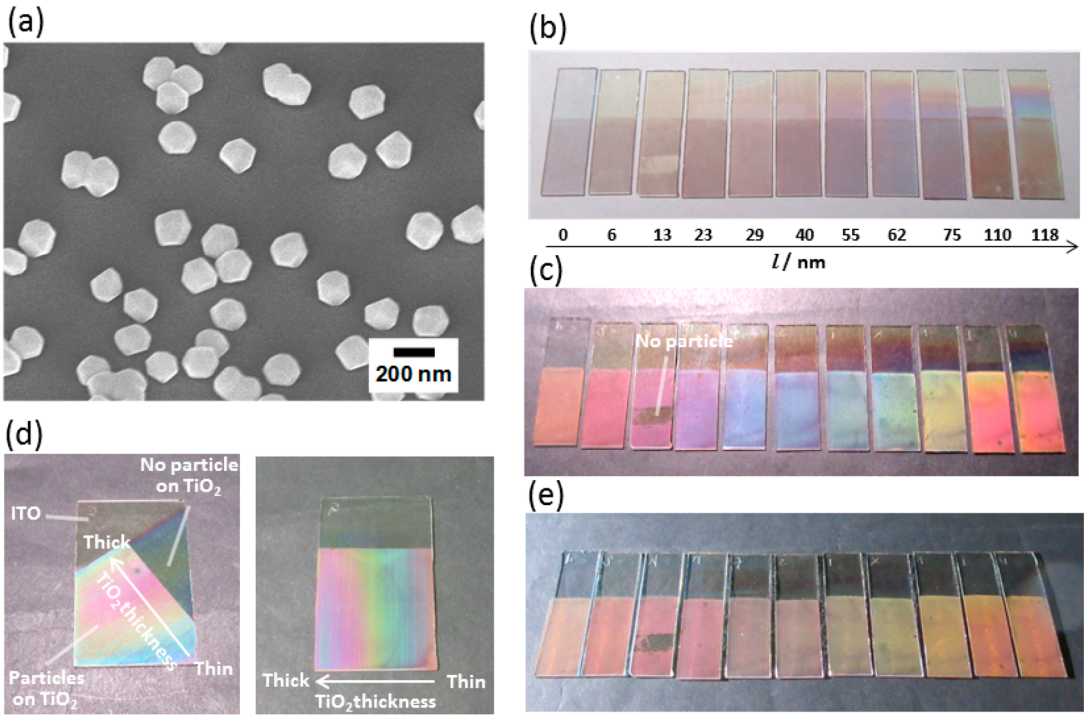

Figure 1. (a) Typical SEM image of Au nanoparticles deposited on a TiO_2 film. (b) Photograph of the substrates coated with TiO_2 films of different thickness l, on which Au nanoparticles are adsorbed, with a white background under ambient light for showing transmission colors and (c–e) those with a black background under strong white light for showing scattering colors, at $\theta_i \sim$ (b–d) 0° or (e) 75°, $\theta_d \sim 20°$. (d) Thickness-gradient TiO_2 films were used.

nanocubes on a TiO_2 film.[23] However, Ag nanoparticles suffer from oxidation, resulting in morphology changes and color degradation. Such degradation is accelerated by PICS when the Ag nanoparticles are in contact with semiconductor and irradiated with strong visible light.[34] Although the PICS effect could be suppressed by replacing the semiconductor substrate[30] or protecting the nanoparticles,[35] these may affect LSPR properties of the nanoparticles and change the colors. A more convenient way is to replace Ag with chemically more stable Au. However, Au nanoparticles exhibit LSPR only at wavelengths longer than ca. 500 nm,[1] so that full-color plasmonic scattering is not possible. We therefore exploit dielectric, nonplasmonic Mie scattering from Au nanoparticles of the size comparable to light wavelength for blue light scattering to achieve full-color scattering with stable Au nanoparticles in the present work.

We deposited cuboctahedral Au nanoparticles of ~150 nm in size on a TiO_2/ITO film (Scheme 1a). Au nanoparticles of this size exhibit strong Mie scattering as well as intense plasmonic scattering in the visible range. Actually, it is known that Mie scattering is significant when the size parameter $2\pi r/\lambda$, where r and λ are the particle diameter and light wavelength, respectively,[36] is larger than unity, and the value of the parameter for the present Au nanoparticles is around 1.3–2.3 in the visible range. Plasmonic scattering intensity is also enhanced as the particle size increases, and Au nanoparticles

DOI: 10.1021/acsanm.9b00990
ACS Appl. Nano Mater. XXXX, XXX, XXX–XXX

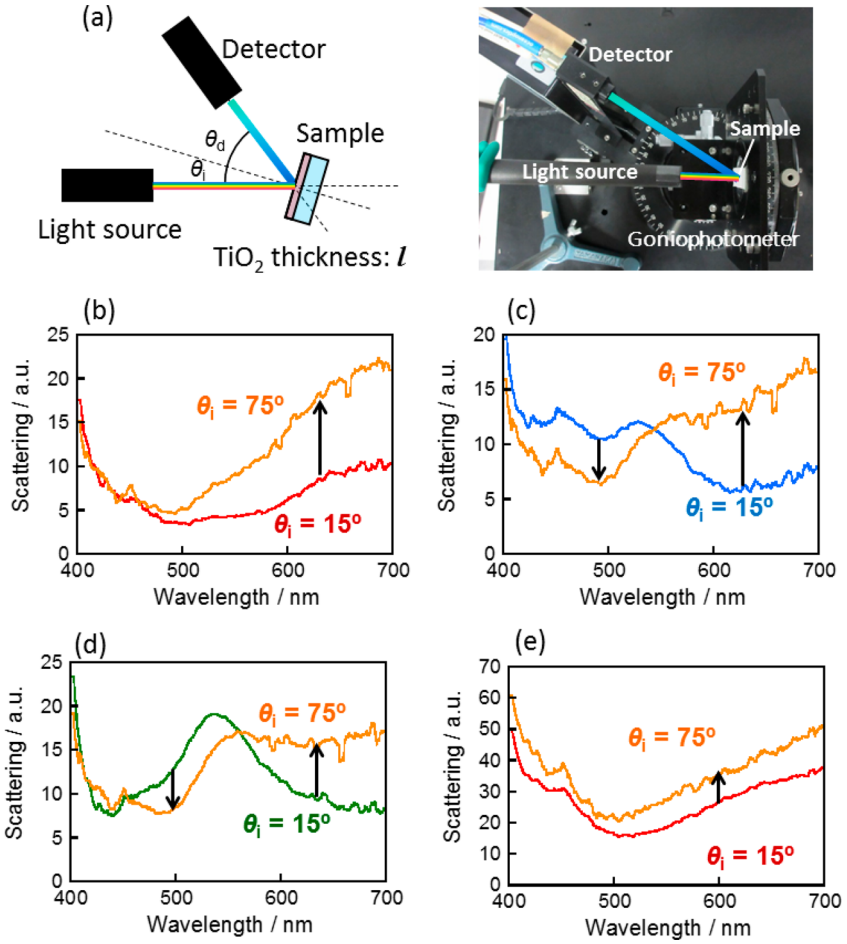

Figure 2. (a) Setup for measurements of angle-dependent scattering spectra. Scattering spectra of the plasmonic samples with TiO_2 thickness l of (b) 6, (c) 29, (d) 62, and (e) 118 nm collected at different incident angles (θ_i = 15° and 75°) and a constant detection angle (θ_d = 0°).

are known to exhibit significant plasmonic scattering if their size is ~50 nm or larger.[2] In addition, if a sufficiently high and bulky plasmonic nanoparticle (typically $r \sim 100$ nm or larger) is in contact with a highly refractive substrate like TiO_2, its plasmon resonance mode splits into full-surface mode, in which electron oscillation and plasmonic electric field spread over the particle surface, and interface mode, in which those are localized at the particle−substrate interface, and the nanoparticle exhibits strong scattering at different wavelengths.[24,26] In the present work, we exploit those three types of scattering based on the Mie resonance, full-surface mode, and interface mode for different scattering colors and enhance or suppress each scattering mode by utilizing Fabry−Pérot interference in the thickness-controlled TiO_2 layer (Scheme 1b). The present system is very simple and can exhibit various scattering colors including blue, green, and red, without changing the size and shape of Au nanoparticles. It can also exhibit broad-band scattering, which allows application to a transparent projection screen.

2. RESULTS AND DISCUSSION

2.1. Appearance of the Films. We prepared a TiO_2 thin film (thickness l = 6−118 nm) on an indium−tin oxide (ITO, thickness = 150 nm)-coated glass substrate. Au nanocubes (~55 nm) were adsorbed onto the TiO_2 film and grown into large polyhedral Au nanoparticles (~150 nm). A typical scanning electron microscope (SEM) image of the prepared particles is shown in Figure 1a. Most of the polyhedrons have a cuboctahedral shape with eight triangular Au{111} facets and six square Au{100} facets. The colors of the particles on TiO_2-coated substrates with different thicknesses were observed for different incident angle (θ_i) and detection angle (θ_d). The results are shown in Figure 1b,c. The color of the light transmitted through the samples, which was observed on a white background, was a reddish one regardless of the TiO_2 thickness (Figure 1b). We also observed the color of the light scattered from the samples on a black background under strong white light, at θ_i of ~0° and θ_d of ~20°, and found that its color was dependent on the TiO_2 thickness even though the particles were almost monodisperse (Figure 1c). The color changed in order of red, blue, green, and yellow and reverted to red as the thickness increased from 6 to 118 nm. The multicolor scattering was also exhibited by the nanoparticles on a thickness-gradient TiO_2 film ($l \sim 6$−150 nm, Figure 1d).

After removal of the nanoparticles from the TiO_2 surface by scratching, no scattered light was observed as shown in Figure 1c,d. When either the incident angle or detection angle was large (e.g., $\theta_i \sim 75°$, $\theta_d \sim 20°$ (Figure 1e) or $\theta_i \sim 0°$, $\theta_d \sim 75°$), the scattering color was an orangish to reddish one, regardless of the TiO_2 thickness. Although the multicolor scattering can be observed for the front side, the color was a reddish one at any θ_i and θ_d for the back side. As described above, Au nanoparticles are essential for the multicolor scattering, which is shown only at low θ_i, and the color depends on the TiO_2

DOI: 10.1021/acsanm.9b00990
ACS Appl. Nano Mater. XXXX, XXX, XXX−XXX

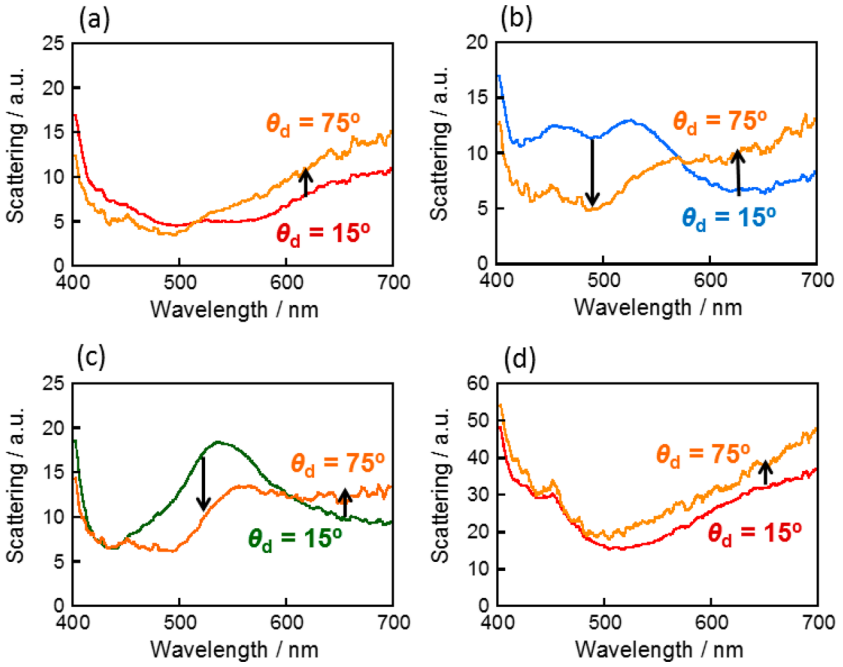

Figure 3. Scattering spectra of the plasmonic samples with TiO_2 thickness l of (a) 6, (b) 29, (c) 62, and (d) 118 nm measured at a constant incident angle ($\theta_i = 0°$) and different detection angles ($\theta_d = 15°$ and 75°).

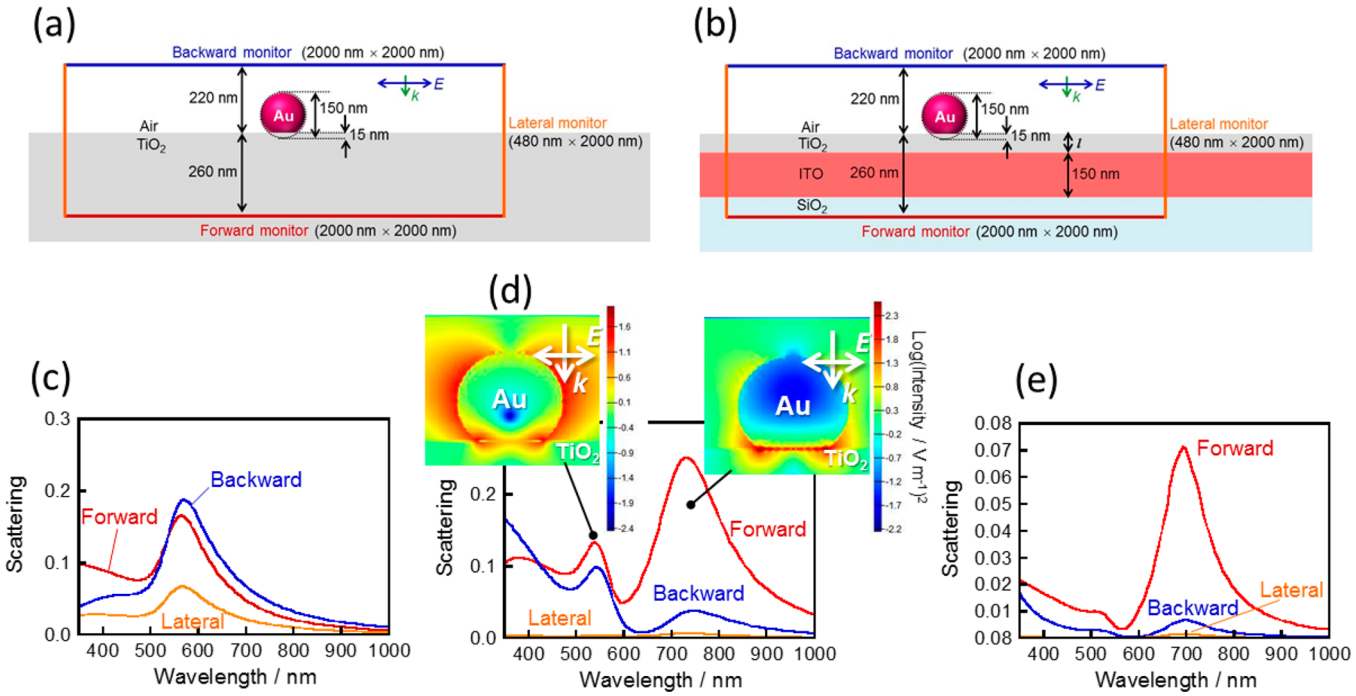

Figure 4. Calculation models for (a) a Au nanoparticle on bulk TiO_2 and (b) that on a TiO_2 thin layer. Backward (blue curves), forward (red curves), and lateral (orange curves) scattering spectra of (c) an isolated 150 nm Au nanoparticle in air, (d) a 150 nm Au nanoparticle on bulk TiO_2, and (e) a 100 nm Au nanoparticle on bulk TiO_2. Insets in panel d represent electric field distributions monitored at the plane parallel to the incident plane and passed through the nanoparticle center.

thickness in a periodic manner, suggesting that plasmonic scattering and Fabry−Pérot interference of light reflected at the TiO_2−air, TiO_2−ITO, and ITO−glass interfaces contribute to the multicolor scattering.

2.2. Scattering Spectra. To investigate effects of θ_i and θ_d on the scattering color in more detail, we collected scattering spectra of the samples using a goniophotometer shown in Figure 2a. The spectra obtained at $\theta_i = 15°$ and $\theta_d = 0°$ of the samples with 6, 29, 62, and 118 nm thick TiO_2, which show red, blue, green, and red colors, respectively, are shown in Figure 2b−e (red, blue, green, and red curves). Each spectrum was smoothed with a 20-point moving average (from $\lambda - 2.5$ to $\lambda + 2.5$ in nm). The main scattering bands are located at ∼700, ∼450, ∼530, and ∼700 nm, respectively, in good agreement with the scattering colors observed by the naked eye. All the 10 samples with different TiO_2 thicknesses showed

DOI: 10.1021/acsanm.9b00990
ACS Appl. Nano Mater. XXXX, XXX, XXX−XXX

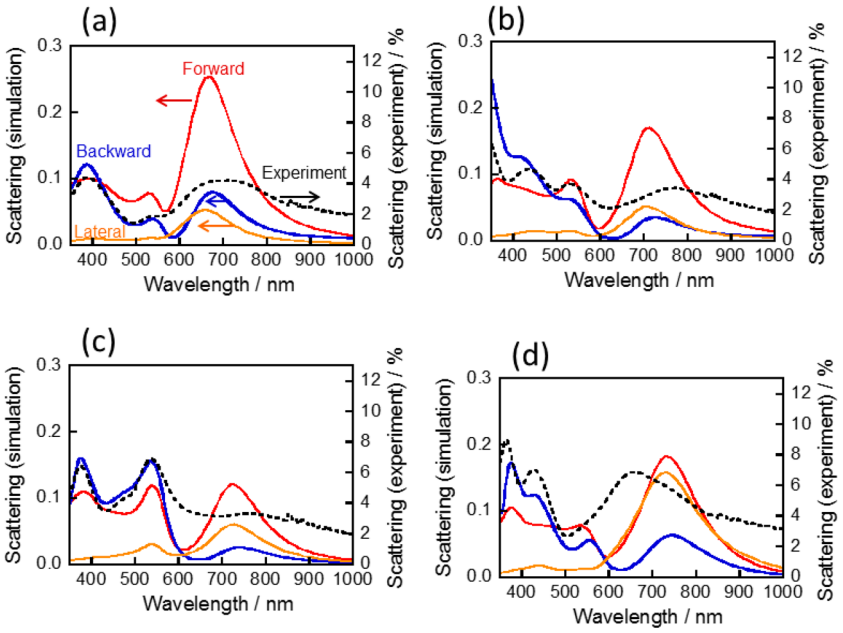

Figure 5. Calculated forward (red curves), backward (blue curves), and lateral (orange curves) scattering spectra and experimental backward scattering spectra (black dashed curves) of Au nanoparticle (150 nm)-modified TiO_2 substrates with l of (a) 6, (b) 30, (c) 60, and (d) 120 nm.

at most three scattering bands at ~450, ~530, and ~700 nm with different intensities, resulting in various scattering colors.

The orange curves in Figure 2b–e represent scattering spectra measured at $\theta_i = 75°$ and $\theta_d = 0°$. All those spectra are characterized by the scattering band at >500 nm, which is responsible for the orangish or reddish scattering color shown in Figure 1e. Effects of the detection angle θ_d on the scattering spectra were also examined at $\theta_i = 0°$ and $\theta_d = 15°–75°$ (Figure 3). The increase in θ_d also resulted in suppression of the thickness-dependent scattering colors and appearance of the orange-red scattering band. From spectra collected at various incident and detection angles, we conclude that the multicolor scattering can be seen at $\theta_i < ~40°$ and $\theta_d < ~40°$ and that it is ascribed to thickness-dependent modulation of the intensity ratio of the three scattering bands at ~450, ~530, and ~700 nm.

2.3. Spectral Simulations. For an explanation of the aforementioned scattering behaviors to be more precise, we performed the simulation of forward, lateral, and backward scattering spectra on the basis of a finite-difference time-domain (FDTD) method. Calculation models are shown in Figure 4a,b. Because the nanoparticles are not perfect cuboctahedrons and have some different orientations, a spherical Au nanoparticle was used for calculations. We also calculated scattering spectra for the Au nanoparticle in air by replacing the TiO_2 substrate in Figure 4a with air (Figure 4c). Only one scattering peak due to LSPR is observed at ca. 570 nm in each spectrum for the nanoparticle in air. The intensity of the backward scattering light is close to that of the forward scattering light for the plasmonic Au nanoparticle with the size of 150 nm. The scattering observed at wavelengths shorter than 500 nm is ascribed to nonplasmonic Mie scattering because the intensity of the forward scattering is higher than that of the backward scattering, and it increases with shortening wavelength, as is the case for typical spherical particles.[37,38] Scattering spectra for the Au nanoparticle on bulk TiO_2 are shown in Figure 4d. Each spectrum is characterized by two LSPR peaks at ~540 and 700–800 nm, which are assigned to the aforementioned full-surface and interface modes, respectively,[26] on the basis of electric field distributions shown as insets. Therefore, we conclude that the scattering peaks observed at ~450, ~530, and 700 nm in Figure 2b–e correspond to nonplasmonic Mie scattering, plasmonic full-surface mode, and plasmonic interface mode, respectively.

It is noteworthy that the interface mode tends to scatter light forward much more than backward. This is because scattered light preferentially propagates into a medium with a high-refractive index (TiO_2 in this case) when LSPR takes place at the interface between two different media.[22,39–42] The lateral scattering (scattering components roughly normal to k vector) intensity is also suppressed. Those spectra indicate that the Au nanoparticle ensemble on TiO_2 serves as a color router that emits red light selectively in the forward direction. This color routing function is not expected for smaller Au nanoparticles (e.g., 100 nm diameter, Figure 4e) because light scattered by Mie and full-surface modes also propagates into TiO_2 as is the case for interface mode, and the wavelength selectivity is lost.

Next we calculated forward, backward, and lateral scattering spectra of a Au nanoparticle on a TiO_2 thin film (l = 6, 30, 60, and 118 nm) by using the model depicted in Figure 4b, and the results are shown in Figure 5 as red, blue, and orange curves, respectively. Experimentally observed backward scattering spectra taken by a spectrophotometer are also shown (black dashed curves). The shapes of the experimental spectra were well reproduced by the calculation (blue solid curves), especially in the wavelength range <550 nm. The three scattering bands corresponding to blue, green, and red scatterings are observed at around 400, 550, and 700 nm, and the intensity ratio is modulated by the changes of the film thickness. Note that similar spectral features were observed when the Au nanosphere was replaced with a cuboctahedral nanoparticle whose volume is the same as that of the nanosphere (Figure S1).

2.4. Interference of the Films. We therefore speculated that the Fabry–Pérot interference in the TiO_2 and ITO layers

DOI: 10.1021/acsanm.9b00990
ACS Appl. Nano Mater. XXXX, XXX, XXX–XXX

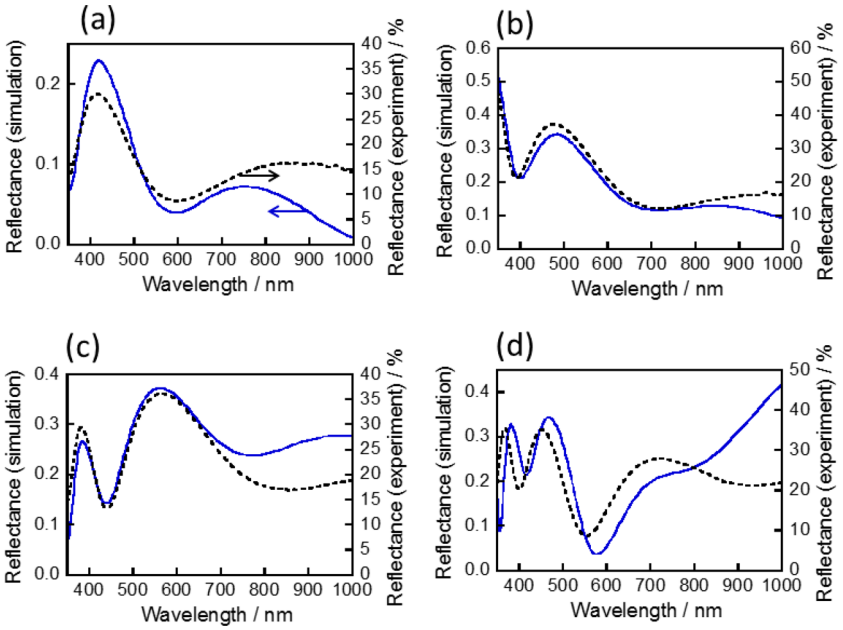

Figure 6. Calculated (blue solid curves) and experimental (black dashed curves) reflection spectra of TiO_2 substrate with l of (a) 6, (b) 30, (c) 60, and (d) 120 nm without Au nanoparticles.

is responsible for the thickness-dependent modulation of the backward scattering and examined the hypothesis by experimentally measuring and theoretically calculating the reflection spectra of the TiO_2/ITO bilayer on a glass plate without Au nanoparticles. Figure 6 shows reflection spectra obtained by experiments (black dashed curves) and calculations (blue solid curves) of the substrate. The calculated spectra are in good accordance with the experimental ones in shape. As the TiO_2 thickness increases, the wavelength of constructive interference (i.e., reflectance peak) is red-shifted in the order of purple, blue, green, and red regions. Forward scattering from the particle is reflected backward, and backward scattering is enhanced at the constructive wavelength.

The Fabry−Pérot interference thus explains the thickness-dependent scattering colors well, but not perfectly. Actually, experimentally observed scattering of each sample in the >550 nm region was more intense than that expected from the simulation, as Figure 5 shows. This should be attributed to difference of the calculation model from the experimentally prepared nanoparticles. Some particles aggregate as Figure 1a shows and exhibit a collective mode scattering in the long wavelength region. To address this point, we calculated backward scattering spectra for a particle dimer model with 10 nm interparticle gap (Figure S2). The scattering intensity of the dimer is significantly higher than that of the single nanosphere in the >550 nm region for light polarized along the interparticle axis. An additional explanation is secondary scattering: scattered light from a nanoparticle partially propagates through the TiO_2 and ITO layers, and the propagating light is scattered by other particles. This effect is peculiar to the system with a thin layer and is deeply related to the interface mode. Because red light is scattered by the interface mode at the particle−film interface, it should be easier to enter the thin film in comparison with blue light and green light, which are scattered by other modes. In addition, the interface site is more accessible to the propagating light than the other sites, so that the secondary scattering of the propagating light by the interface mode is more likely to occur than that by the other modes. The secondary scattering is therefore responsible for the scattering enhancement in the >550 nm range. It also enhances lateral scattering and accounts for the thickness-independent reddish scattering at large θ_d shown in Figure 1e.

2.5. Transparent Projection Screen. Finally, we fabricated a transparent projection screen on the basis of the above results. The screen has to scatter blue, green, and red light for full-color projection. We therefore used the substrate with 30 nm thick TiO_2 because it reflects blue light strongly because of Fabry−Pérot interference. Then the Au nanoparticles shown in Figure 1a were deposited on the TiO_2 layer and grown further in a growth solution into Au nanoparticles with diameter of ca. 200 nm (Figure 7a). We designed the sample to scatter blue, green, and red light in the backward direction at similar intensities. As mentioned above, scattering of blue light is rather difficult for plasmonic nanoparticles. Therefore, backward scattering of blue light was enhanced by the optical interference. Meanwhile, red backward scattering derived from interface mode was suppressed by leading the red scattering light to the forward direction. The backward scattering spectrum thus obtained is shown in Figure 7b. Strong scattering was observed in the whole visible region as a consequence of Mie scattering enhanced by the optical interference (400−500 nm), full surface mode (~560 nm), and interface mode (~800 nm). Various color images were projected by an LCD projector onto the projection screen thus prepared (Figure 7c). Although the screen was visually transparent under ambient light, the color images were clearly shown on the screen. It is noteworthy that white and blue color scatterings, which have been difficult to exhibit by Au nanoparticles, are clearly shown by the present screen.

3. CONCLUSIONS

Scattering behaviors of the relatively large Au nanoparticles based on nonplasmonic Mie scattering and two separated LSPR modes (full-surface and interface modes) were

DOI: 10.1021/acsanm.9b00990
ACS Appl. Nano Mater. XXXX, XXX, XXX−XXX

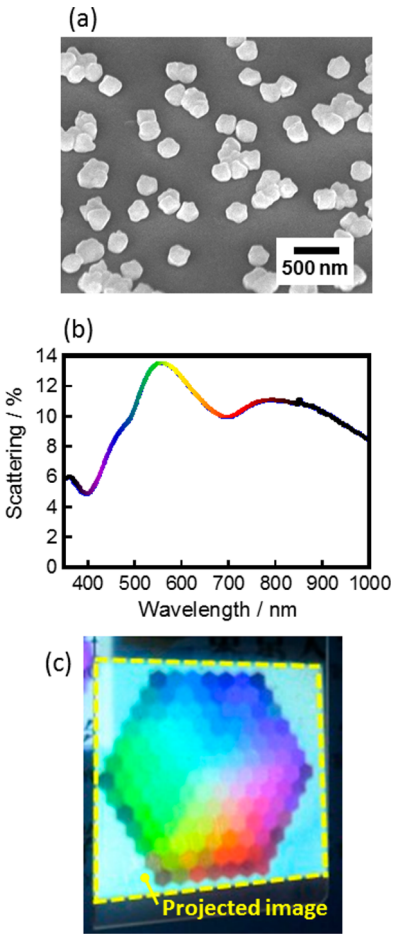

Figure 7. (a) Typical SEM image of Au nanoparticles used for the transparent projection screen. (b) Backward scattering spectrum of the projection screen composed of the Au nanoparticles and a TiO_2 substrate with l of ∼30 nm. (c) Photograph of a color image projected on the screen.

modulated by Fabry−Pérot interference so that full-color scattering was achieved and a transparent projection screen was developed. Because those plasmonic films are stable because of Au and exhibit blue and white scattering colors, which have been difficult to exhibit by Au nanoparticles, those films should be more practical than those based on Ag nanoparticles.[22−24,27,30] If those films are combined with the PICS technology, a photocatalytic self-cleaning function could be added. Because of their unique scattering colors dependent on the incident and detection angles, those plasmonic films are potentially applicable to anticounterfeiting. Because all the fabrication processes are based on chemical methods (i.e., bottom-up techniques), the present technique would lead to cost-effective, scattering-based plasmonic coloring for large area.

4. EXPERIMENTAL SECTION

An anatase TiO_2 thin layer was deposited on a smooth ITO (thickness: 150 nm)-coated glass substrate (Kuramoto) by a spray pyrolysis method from titanium diisopropoxide bis(acetylacetonate) (75 wt % in 2-propanol, Sigma-Aldrich) diluted with 2-propanol (1:18 v/v) at 500 °C (spray pressure: 0.12 MPa; spray time: 1 s; the number of sprays: 1−11 times with an interval of 1 min). The TiO_2 thickness was determined from its reflectance spectrum with reference to theoretically calculated spectra. Au nanocubes (size: ∼55 nm) were synthesized by a seed-mediated growth method according to the literature[43] with modifications. The nanocubes were adsorbed onto the TiO_2 surface by immersing the substrate in the nanocube solution diluted with ethanol (3:1 v/v) overnight. The adsorbed nanocubes were grown into cuboctahedral Au nanoparticles (∼150 nm) in a growth solution, which was prepared by adding an aqueous solution of ascorbic acid (0.1 M, 200 μL) to a mixed solution of cetyltrimethylammonium bromide (CTAB) (0.1 M, 10.72 mL), cetyltrimethylammonium chloride (CTAC) (0.1 M, 8.8 mL), and hydrogen tetrachloroaurate(III) tetrahydrate (0.05 M, 80 μL) with stirring for 2 h. The nanoparticles were grown further by repeating the procedure for preparation of a transparent projection screen.

Reflectance and scattering spectra were obtained by a Jasco V-670 spectrometer equipped with an ISN-723 integrating sphere. A goniophotometer equipped with a fiber-optic Xe lamp (Asahi Spectra, LAX-102) and a high-resolution miniature fiber-optic spectrophotometer (Ocean Optics, HR4000CG) was used for angle-resolved scattering measurements.

Spectral simulations were performed by the FDTD method using FDTD solutions (Lumerical Solutions) with calculation models shown in Figure 4a,b. A 150 nm spherical Au particle whose bottom is truncated by 15 nm was placed on bulk TiO_2 or a substrate composed of a TiO_2 layer with thickness of l, an ITO layer with thickness of 150 nm, and a glass plate. The 15 nm truncation gives the contact area of ∼6400 nm^2, which is the value in between the values expected for the cuboctahedron of the same volume, 8100 nm^2 (square facet) and 3500 nm^2 (triangular facet). The other area was filled with air (n = 1). Thus, the height of the particle is 135 nm, and the Au−TiO_2 interface is a circle with diameter of 90 nm. Light was incident from the air (front) side of the substrate. The simulation area close to the AuNP was meshed in a three-dimensional box (480 × 480 × 480 nm^3) composed of 2 nm cubic cells. The auto shut-off parameter was set to 10^{-5}.

Light scattering (without normal reflection and transmission) was detected by six monitors. Backward and forward monitors (2000 nm × 2000 nm) parallel to the substrate were placed 220 and 260 nm away from the air−TiO_2 interface toward the air and substrate sides, respectively. The center of the monitor is aligned with that of the particle. Scattering light detected by these monitors at the air and substrate sides was regarded as backward and forward scattering, respectively. Lateral scattering components except for forward and backward scattering were detected by four lateral monitors (480 nm × 2000 nm) parallel to the incident axis. Two of them are parallel to the E vector, and the other two are normal.

■ ASSOCIATED CONTENT

Supporting Information

The Supporting Information is available free of charge on the ACS Publications website at DOI: 10.1021/acsanm.9b00990.

Simulated spectra for a cuboctahedron model (Figure S1) and a nanosphere dimer model (Figure S2) (PDF)

■ AUTHOR INFORMATION

Corresponding Authors

*E-mail: nishi-h@iis.u-tokyo.ac.jp.

*E-mail: tatsuma@iis.u-tokyo.ac.jp.

ORCID

Tetsu Tatsuma: 0000-0001-8738-9837

Notes

The authors declare no competing financial interest.

■ ACKNOWLEDGMENTS

This work was supported in part by a Grant-in-Aid for Scientific Research (A) (No. JP16H02082) and a Grant-in-Aid for Early-Career Scientists (No. JP18K14186) from the Japan Society for the Promotion of Science (JSPS).

DOI: 10.1021/acsanm.9b00990
ACS Appl. Nano Mater. XXXX, XXX, XXX−XXX

REFERENCES

(1) Link, S.; Wang, Z. L.; El-Sayed, M. A. Alloy Formation of Gold−Silver Nanoparticles and the Dependence of the Plasmon Absorption on Their Composition. *J. Phys. Chem. B* **1999**, *103*, 3529−3533.

(2) Jain, P. K.; Lee, K. S.; El-Sayed, I. H.; El-Sayed, M. A. Calculated Absorption and Scattering Properties of Gold Nanoparticles of Different Size, Shape, and Composition: Applications in Biological Imaging and Biomedicine. *J. Phys. Chem. B* **2006**, *110*, 7238−7248.

(3) Lee, K.-S.; El-Sayed, M. A. Gold and Silver Nanoparticles in Sensing and Imaging: Sensitivity of Plasmon Response to Size, Shape, and Metal Composition. *J. Phys. Chem. B* **2006**, *110*, 19220−19225.

(4) Njoki, P. N.; Lim, I.-I. S.; Mott, D.; Park, H.-Y.; Khan, B.; Mishra, S.; Sujakumar, R.; Luo, J.; Zhong, C.-J. Size Correlation of Optical and Spectroscopic Properties for Gold Nanoparticles. *J. Phys. Chem. C* **2007**, *111*, 14664−14669.

(5) Kim, F.; Song, J. H.; Yang, P. Photochemical Synthesis of Gold Nanorods. *J. Am. Chem. Soc.* **2002**, *124*, 14316−14317.

(6) Millstone, J. E.; Hurst, S. J.; Métraux, G. S.; Cutler, J. I.; Mirkin, C. A. Colloidal Gold and Silver Triangular Nanoprisms. *Small* **2009**, *5*, 646−664.

(7) Fang, C.; Shao, L.; Zhao, Y.; Wang, J.; Wu, H. A Gold Nanocrystal/Poly(dimethylsiloxane) Composite for Plasmonic Heating on Microfluidic Chips. *Adv. Mater.* **2012**, *24*, 94−98.

(8) Gluodenis, M.; Foss, C. A., Jr. The Effect of Mutual Orientation on the Spectra of Metal Nanoparticle Rod−Rod and Rod−Sphere Pairs. *J. Phys. Chem. B* **2002**, *106*, 9484−9489.

(9) Fan, P.; Zhong, M.; Li, L.; Schmitz, P.; Lin, C.; Long, J.; Zhang, H. Sequential Color Change on Copper Surfaces via Micro/Nano Structure Modification Induced by a Picosecond Laser. *J. Appl. Phys.* **2013**, *114*, 083518.

(10) Vorobyev, A. Y.; Guo, C. Direct Femtosecond Laser Surface Nano/Microstructuring and its Applications. *Laser Photon. Rev.* **2013**, *7*, 385−407.

(11) Fan, P.; Zhong, M.; Li, L.; Schmitz, P.; Lin, C.; Long, J.; Zhang, H. Angle-Independent Colorization of Copper Surfaces by Simultaneous Generation of Picosecond-Laser-Induced Nanostructures and Redeposited Nanoparticles. *J. Appl. Phys.* **2014**, *115*, 124302.

(12) Guay, J.-M.; Lesina, A. C.; Côté, G.; Charron, M.; Poitras, D.; Ramunno, L.; Berini, P.; Weck, A. Laser-Induced Plasmonic Colours on Metals. *Nat. Commun.* **2017**, *8*, 16095.

(13) Kumar, K.; Duan, H.; Hegde, R. S.; Koh, S. C. W.; Wei, J. N.; Yang, J. K. W. Printing Colour at the Optical Diffraction Limit. *Nat. Nanotechnol.* **2012**, *7*, 557−561.

(14) Li, Z.; Clark, A. W.; Cooper, J. M. Dual Color Plasmonic Pixels Create a Polarization Controlled Nano Color Palette. *ACS Nano* **2016**, *10*, 492−498.

(15) Lu, B.-R.; Xu, C.; Liao, J.; Liu, J.; Chen, Y. High-Resolution Plasmonic Structural Colors from Nanohole Arrays with Bottom Metal Disks. *Opt. Lett.* **2016**, *41*, 1400−1403.

(16) Wang, H.; Wang, X.; Yan, C.; Zhao, H.; Zhang, J.; Santschi, C.; Martin, O. J. F. Full Color Generation Using Silver Tandem Nanodisks. *ACS Nano* **2017**, *11*, 4419−4427.

(17) *Nobel Lectures, Chemistry 1922−1941*; Elsevier: Amsterdam, 1966.

(18) Jin, R.; Cao, Y.; Mirkin, C. A.; Kelly, K. L.; Schatz, G. C.; Zheng, J. G. Photoinduced Conversion of Silver Nanospheres to Nanoprisms. *Science* **2001**, *294*, 1901−1903.

(19) Chen, T.; Reinhard, B. M. Assembling Color on the Nanoscale: Multichromatic Switchable Pixels from Plasmonic Atoms and Molecules. *Adv. Mater.* **2016**, *28*, 3522−3527.

(20) Freestone, I.; Meeks, N.; Sax, M.; Higgitt, C. The Lycurgus Cup — A Roman Nanotechnology. *Gold Bull.* **2007**, *40*, 270−277.

(21) Barber, D. J.; Freestone, I. C. An Investigation of the Origin of the Colour of the Lycurgus Cup by Analytical Transmission Electron Microscopy. *Archaeometry* **1990**, *32*, 33−45.

(22) Saito, K.; Tatsuma, T. Asymmetric Three-Way Plasmonic Color Routers. *Adv. Opt. Mater.* **2015**, *3*, 883−887.

(23) Saito, K.; Tatsuma, T. Transparent Projection Screen Based on Plasmonic Ag Nanocubes. *Nanoscale* **2015**, *7*, 20365−20368.

(24) Okumura, A.; Saito, K.; Tatsuma, T. Asymmetric Optical Properties of Photocatalytically Deposited Plasmonic Silver Nanoparticles. *Phys. Chem. Chem. Phys.* **2016**, *18*, 7007−7010.

(25) Saito, K.; Tatsuma, T. Control of Asymmetric Scattering Behavior of Plasmonic Nanoparticle Ensembles. *ACS Photonics* **2016**, *3*, 1782−1786.

(26) Tanabe, I.; Tatsuma, T. Plasmonic Manipulation of Color and Morphology of Single Silver Nanospheres. *Nano Lett.* **2012**, *12*, 5418−5421.

(27) Saito, K.; Tanabe, I.; Tatsuma, T. Site-Selective Plasmonic Etching of Silver Nanocubes. *J. Phys. Chem. Lett.* **2016**, *7*, 4363−4368.

(28) Tian, Y.; Tatsuma, T. Mechanisms and Applications of Plasmon-Induced Charge Separation at TiO_2 Films Loaded with Gold Nanoparticles. *J. Am. Chem. Soc.* **2005**, *127*, 7632−7637.

(29) Tatsuma, T.; Nishi, H.; Ishida, T. Plasmon-Induced Charge Separation: Chemistry and Wide Applications. *Chem. Sci.* **2017**, *8*, 3325−3337.

(30) Saito, K.; Setoura, K.; Ito, S.; Miyasaka, H.; Mitsuda, Y.; Tatsuma, T. Plasmonic Control and Stabilization of Asymmetric Light Scattering from Ag Nanocubes on TiO_2. *ACS Appl. Mater. Interfaces* **2017**, *9*, 11064−11072.

(31) Hsu, C. W.; Zhen, B.; Qiu, W.; Shapira, O.; DeLacy, B. G.; Joannopoulos, J. D.; Soljačić, M. Transparent Displays Enabled by Resonant Nanoparticle Scattering. *Nat. Commun.* **2014**, *5*, 3152.

(32) Ye, Y.; Chen, T.; Zhen, J.; Xu, C.; Zhang, J.; Li, H. Resonant Scattering of Green Light Enabled by Ag@TiO_2 and its Application in a Green Light Projection Screen. *Nanoscale* **2018**, *10*, 2438−2446.

(33) Ye, Y.; Chen, T. P. Selective Scattering of Blue and Red Light Based on Silver and Gold Nanocubes. *ECS J. Solid State Sci. Technol.* **2019**, *8*, R51−R57.

(34) Ohko, Y.; Tatsuma, T.; Fujii, T.; Naoi, K.; Niwa, C.; Kubota, Y.; Fujishima, A. Multicolor Photochromism of TiO_2 Films Loaded with Ag Nanoparticles. *Nat. Mater.* **2003**, *2*, 29−31.

(35) Naoi, K.; Ohko, Y.; Tatsuma, T. Switchable Rewritability of Ag-TiO_2 Nanocomposite Films with Multicolor Photochromism. *Chem. Commun.* **2005**, 1288−1290.

(36) Graaff, R.; Aarnoudse, J. G.; Zijp, J. R.; Sloot, P. M. A.; de Mul, F. F. M.; Greve, J.; Koelink, M. H. Reduced Light-Scattering Properties for Mixtures of Spherical Particles: a Simple Approximation Derived from Mie Calculations. *Appl. Opt.* **1992**, *31*, 1370−1376.

(37) Bohren, C. F.; Huffman, D. R. *Absorption and Scattering of Light by Small Particles*; John Wiley & Sons: New York, 2007.

(38) Anderson, L. J. E.; Mayer, K. M.; Fraleigh, R. D.; Yang, Y.; Lee, S.; Hafner, J. H. Quantitative Measurements of Individual Gold Nanoparticle Scattering Cross Sections. *J. Phys. Chem. C* **2010**, *114*, 11127−11132.

(39) Lukosz, W.; Kunz, R. E. Light Emission by Magnetic and Electric Dipoles Close to a Plane Interface. I. Total Radiated Power. *J. Opt. Soc. Am.* **1977**, *67*, 1607−1615.

(40) Mertz, J. Radiative Absorption, Fluorescence, and Scattering of a Classical Dipole Near a Lossless Interface: a Unified Description. *J. Opt. Soc. Am. B* **2000**, *17*, 1906−1913.

(41) Shegai, T.; Chen, S.; Miljković, V. D.; Zengin, G.; Johansson, P.; Käll, M. A Bimetallic Nanoantenna for Directional Colour Routing. *Nat. Commun.* **2011**, *2*, 481.

(42) Schmid, M.; Klenk, R.; Lux-Steiner, M. C.; Topič, M.; Krč, J. Modeling Plasmonic Scattering Combined with Thin-Film Optics. *Nanotechnology* **2011**, *22*, 025204.

(43) Eguchi, M.; Mitsui, D.; Wu, H.-L.; Sato, R.; Teranishi, T. Simple Reductant Concentration-Dependent Shape Control of Polyhedral Gold Nanoparticles and Their Plasmonic Properties. *Langmuir* **2012**, *28*, 9021−9026.

DOI: 10.1021/acsanm.9b00990
ACS Appl. Nano Mater. XXXX, XXX, XXX−XXX